THE JOURNAL OF BIOLOGICAL CHEMISTRY VOL. 286, NO. 50, pp. 43549–43558, December 16, 2011

Compensatory Regulation of Dopamine after Ablation of the Tyrosine Hydroxylase Gene in the Nigrostriatal Projection*[S]

Received for publication, July 20, 2011, and in revised form, October 6, 2011 Published, JBC Papers in Press, October 25, 2011, DOI 10.1074/jbc.M111.284729

Hirofumi Tokuoka[‡1], Shin-ichi Muramatsu[§], Chiho Sumi-Ichinose[¶], Hiroaki Sakane[‡], Masayo Kojima[‡], Yoshinori Aso[‡], Takahide Nomura[¶], Daniel Metzger[‖‡‡], and Hiroshi Ichinose[‡2]**

*From the [‡]Department of Life Science, Graduate School of Bioscience and Biotechnology, Tokyo Institute of Technology, 4259 B-7, Nagatsuta, Midori-ku, Yokohama, 226-8501 Japan, the [§]Division of Neurology, Department of Medicine, Jichi Medical University, Tochigi 329-0498, Japan, the [¶]Department of Pharmacology, School of Medicine, Fujita Health University, Toyoake, Aichi 470-1192, Japan, the [‖]Institut de Génétique et de Biologie Moléculaire et Cellulaire, Illkirch F-67400, France, **CNRS, Illkirch, France , and the [‡‡]Université Louis Pasteur, Strasbourg F-67000, France*

Background: The tyrosine hydroxylase (TH) gene, essential for dopamine synthesis, is partially ablated in adult nigrostriatal projection.
Results: TH reduction in axon terminals is slower than in soma, and dopamine is better maintained than TH.
Conclusion: Striatal dopamine is compensatorily regulated by axonal TH level and L-DOPA synthesis activity per TH level.
Significance: This regulation has potential relevance to pathogenesis of Parkinson disease and other dopamine-related psychiatric disorders.

The tyrosine hydroxylase (TH; EC 1.14.16.2) is a rate-limiting enzyme in the dopamine synthesis and important for the central dopaminergic system, which controls voluntary movements and reward-dependent behaviors. Here, to further explore the regulatory mechanism of dopamine levels by TH in adult mouse brains, we employed a genetic method to inactivate the *Th* gene in the nigrostriatal projection using the Cre-*loxP* system. Stereotaxic injection of adeno-associated virus expressing Cre recombinase (AAV-Cre) into the substantia nigra pars compacta (SNc), where dopaminergic cell bodies locate, specifically inactivated the *Th* gene. Whereas the number of TH-expressing cells decreased to less than 40% in the SNc 2 weeks after the AAV-Cre injection, the striatal TH protein level decreased to 75%, 50%, and 39% at 2, 4, and 8 weeks, respectively, after the injection. Thus, unexpectedly, the reduction of TH protein in the striatum, where SNc dopaminergic axons innervate densely, was slower than in the SNc. Moreover, despite the essential requirement of TH for dopamine synthesis, the striatal dopamine contents were only moderately decreased, to 70% even 8 weeks after AAV-Cre injection. Concurrently, *in vivo* synthesis activity of L-dihydroxyphenylalanine, the dopamine precursor, per TH protein level was augmented, suggesting up-regulation of dopamine synthesis activity in the intact nigrostriatal axons. Collectively, our conditional *Th* gene targeting method demonstrates two regulatory mechanisms of TH in axon terminals for dopamine homeostasis *in vivo*: local regulation of TH protein amount independent of soma and trans-axonal regulation of apparent L-dihydroxyphenylalanine synthesis activity per TH protein.

The dopaminergic system is important for many brain functions, including voluntary movements (1) and reward-related behaviors (2). The dysfunction of dopaminergic transmission is involved in many neurological and psychiatric disorders, such as Parkinson disease (3), addiction (4), attention deficit hyperactive disorders (5), and schizophrenia (6). Although chronic alterations in the dopaminergic system may be relevant to these disorders, it is still unclear how the dopaminergic system is regulated over days to months. In Parkinson disease, motor symptoms exhibit only after a large loss of striatal dopamine (7), suggesting compensation for the loss of dopamine. Although studies on Parkinson disease have suggested multiple forms of compensatory mechanisms, including enhanced dopamine release and turnover (8, 9, 10, 11), it is not fully understood what cellular and molecular mechanisms underlie the long term regulation of striatal dopamine levels under non-degenerative conditions.

Chronic intervention in the dopamine system has been performed for many years by pharmacological methods although they exhibit limitations related to dose dependence, drug metabolism, and circuit specificity. Gene-targeting methods, including germ line knock-out mice (12–14) and dopamine-deficient mice (15–17), have been generated, but because dopaminergic transmissions are blocked from the early stage of brain development, these methods may induce developmental effects. To explore the regulatory mechanisms of the nigrostriatal dopaminergic system in the adult brain, we generated mice in which dopamine synthesis can be selectively abrogated in a spatio-temporally controlled manner. The nigrostriatal projection is the largest dopaminergic projection in the brain, and the dense dopaminergic axon terminals in the striatum are readily

* This work was supported by Grants-in-aid for Human Frontier Science Program; by Research Grant 18A-2 for Nervous and Mental Disorders from the Ministry of Health, Labor and Welfare of Japan; by KAKENHI from MEXT; by the Nakajima Foundation; and by Core Research for Evolutional Science and Technology, Japan Science and Technology Agency (CREST, JST).
[S] The on-line version of this article (available at http://www.jbc.org) contains supplemental Figs. 1–5.
[1] To whom correspondence may be addressed. Tel.: 81-45-924-5822; Fax: 81-45-924-5807; E-mail: htokuoka@bio.titech.ac.jp.
[2] To whom correspondence may be addressed. Tel.: 81-45-924-5822; Fax: 81-45-924-5807; E-mail: hichinos@bio.titech.ac.jp.

investigated in isolation from their cell bodies and dendrites. Because tyrosine hydroxylase (TH)[3] is the rate-limiting enzyme in dopamine biosynthesis (18), we generated transgenic mice that contain two *loxP* sites flanking the major coding exons of the *TH* gene (floxed *Th* mice).

A microinjection of adeno-associated viral (AAV) vector expressing Cre recombinase (AAV-Cre) (19, 20) into the substantia nigra pars compacta (SNc) of the floxed *Th* mice disrupted the expression of the *Th* gene in a subset of neurons in the SNc of the adult mice. Our biochemical and histochemical analyses suggest two regulatory mechanisms of axonal TH for dopamine homeostasis in the nigrostriatal projection. First, the TH protein level in axon terminals is regulated differently from that in soma. Second, *in vivo* apparent L-DOPA synthesis activity per TH protein level in a given axon is influenced by dopamine synthesis in the neighboring axons, which we propose as trans-axonal regulation of dopamine levels.

EXPERIMENTAL PROCEDURES

Production of Th Floxed Mice, Genotyping—To construct the targeting vector for generating a floxed *Th* allele, a 9.5-kb XhoI-EcoRI genomic DNA segment containing genomic *Th* DNA was isolated from a λ phage 129SV mouse genomic library. The EcoRI site located at the 3′-end was replaced by MluI, a HindIII restriction site was engineered by site-directed mutagenesis between exons 5 and 6, and the SpeI site located between exons 9 and 10 was converted into a NotI site. A *loxP* site and an EcoRV restriction site were inserted into a HindIII site, and a neomycin-resistant cassette, flanked by *loxP* sites, was inserted into a NotI site. The three *loxP* sites in the final targeting vector were in the same orientation (3′ to 5′) (Fig. 1*A*).

Mouse embryonic stem cells were electroporated with the targeting vector, and the homologously recombinated clones were screened by PCR and Southern blot analysis. Embryonic stem clones with three *loxP* sites were selected, and a plasmid expressing Cre DNA recombinase was transiently transfected into the cells. Embryonic stem cells with two *loxP* sites without a neomycin cassette were selected by PCR and used for production of chimeric mice.

The genotypes of mice were identified on mouse ear biopsies by PCR (30 cycles at 94 °C for 30 s, 65 °C for 3 min, and a final extension at 72 °C for 5 min) with primers TH9F (5′-CATTTGCCCAGTTCTCCCAG-3′) and TH10R (5′-AGAGATGCAAGTCCAATGTC-3′). The sizes of the PCR products amplified from the wild-type *Th* allele and from the floxed *Th* allele are 431 and 513 bp, respectively.

For the detection of recombined *Th* alleles, genomic DNA was extracted from the substantia nigra regions of brain slices fixed by paraformaldehyde. The recombined *Th* alleles were detected by PCR (30 cycles at 94 °C for 30 s, 66 °C for 30 s, 72 °C for 1 min 15 s, and a final extension at 72 °C for 5 min) with primers TH5F (5′-AGGCGTATCGCCAGCGCC-3′) and TH10Rb (5′-CCCCAGAGATGCAAGTCCAATGTC-3′). The sizes of the PCR products amplified from the wild-type *Th* allele, floxed *Th* allele, and deleted *Th* allele are 1722, 1886, and 430 bp, respectively.

AAV Vector Construction—We generated two types of AAV-Cre vectors basically as described previously (19). One was the AAV-Cre vector, which contained an expression cassette with a human cytomegalovirus immediate early promoter (CMV promoter), followed by the first intron of human growth hormone, Cre recombinase cDNA, and simian virus 40 polyadenylation signal sequence (SV40 poly(A)), between the inverted terminal repeats of the AAV-2 genome. The other was the AAV-GFP/Cre vector, which contained an expression cassette with a synapsin I promoter (21), followed by AcGFP1 (Clontech), the internal ribosomal entry site, Cre recombinase cDNA, and simian virus 40 polyadenylation signal sequence (SV40 poly(A)), between the inverted terminal repeats of the AAV-1 genome. The two helper plasmids, pHLP19 and pladeno1 (Avigen, Alameda, CA), harbored the AAV *rep* and *cap* genes as well as the E2A, E4, and VA RNA genes of the adenovirus genome, respectively. HEK293 cells were co-transfected with the vector plasmid, pHLP19, and pladeno1 by the calcium phosphate precipitation method. The AAV vectors were then harvested and purified by two rounds of continuous iodoxale ultracentrifugations. Vector titers were determined by quantitative DNA dot-blot hybridization or by quantitative PCR of DNase I-treated vector stocks. We routinely obtained 10^{12} to 10^{13} vector genome copies/ml.

Animals and Stereotaxic Microinjections—Mice were acclimated to and maintained at 25 °C under a 12-h light/dark cycle (light on 08:00–20:00). All animal experiments were performed in accordance with the general guidelines of the Tokyo Institute of Technology. Unilateral injections into the SNc were performed on 12–16-week-old mice that were anesthetized with Nembutal (intraperitoneally) and mounted into a stereotaxic apparatus. The coordinates were 3.0 mm posterior from bregma, 1.0 mm lateral to midline, and 4.0 mm ventral from the dural surface. 1 μl of AAV-Cre or AAV-GFP/Cre (about 10^9 particles) was injected through an injection cannula (28-gauge) with a Hamilton microsyringe driven by a microdialysis pump at a rate of 0.2 μl/min. After microinjection, the injection cannula was left for 2 min before its withdrawal to reduce the efflux of injected liquid along the injection tract. When a cannula was blocked or leaked, the mouse was excluded from the following experiments. The mice were sacrificed at 1, 2, 4, 8, or 16 weeks after microinjection for analyses. We used the uninjected side of a brain as a control side to compare with. $Th^{+/+}$ mice were used as control animals.

Immunohistochemistry—Striatal slices were prepared by transcardial perfusion with saline, followed by 4% paraformaldehyde, 60 mM phosphate buffer, and postfixation overnight. All solutions were used at 4 °C. In some experiments, striatal tissues were dissected and homogenized for Western blot and monoamine assay (see below), and the rest of the brain, including the midbrain with the SNc region, was fixed by immersing in 4% paraformaldehyde, PBS overnight. The fixed brain pieces

[3] The abbreviations used are: TH, tyrosine hydroxylase; AADC, aromatic L-amino acid decarboxylase; AAV, adeno-associated virus; AAV-Cre, adeno-associated virus expressing Cre recombinase; DA, dopamine; DAT, dopamine transporter; DOPAC, 3,4-dihydroxyphenylacetic acid; HVA, homovanillic acid; L-DOPA, L-dihydroxyphenylalanine; vMAT2, vesicular monoamine transporter 2; SNc, substantia nigra pars compacta; 6-OHDA, 6-hydroxydopamine; GBR12909, 1-[2-[bis-(4-fluorophenyl)methoxy]ethyl]-4-(3-phenylpropyl)piperazine dihydrochloride.

were cryoprotected by 30% sucrose, and the coronal slices of 30-μm thickness were cut by a cryostat. The free floating serial coronal sections, from the rostral to the caudal edge of SNc or a part of the striatum, were incubated with rabbit anti-TH antibody (1:10,000; Millipore) or rabbit anti-AADC serum (1:20,000) (12), followed by biotinylated goat anti-rabbit IgG antibody (1:250; Vector Laboratories) and avidin-peroxidase complex (Vectastain ABC kit, Vector Laboratories). Immunocomplexes were visualized by a reaction with 3,3′-diaminobenzidine tetrahydrochloride and 0.003% H_2O_2. Images were taken using an upright microscope (Eclipse E800, Nikon) equipped with a cooled CCD camera (VB-6010, Keyence).

The numbers of TH-positive neurons in the injected and uninjected side SNc were compared using a stereological cell counting method. SNc was defined according to the brain atlas (22). Briefly, one in every three coronal sections covering the whole SNc was selected (typically 12–14 sections) and stained for TH, and magnified images of SNc were taken using a 20× objective lens (numerical aperture 0.5). For each region of interest, images were taken at multiple different focus planes to visualize all cells in the thickness. The number of all TH-positive cells in SNc in each slice was counted manually with ImageJ (National Institutes of Health). Only cells with an apparently visible nucleus were included. The number of all TH-positive neurons from a set of slices was summed (typically 1600–2000 cells in the uninjected side), and the ratio of the number in the injected side to that in the uninjected side was evaluated.

For fluorescence immunohistochemistry, the following secondary antibodies were used: Alexa546-conjugated anti-mouse IgG (1:2,000; Invitrogen) and Alexa633-conjugated anti-rabbit IgG (1:2,000; Invitrogen). Images were taken using the TCS SPE confocal microscope (Leica) with a 63× oil objective lens and excitation lasers of 532 and 635 nm.

For the detection of dopamine, we fixed mice transcardially with 5% glutaraldehyde, and the brain sections made with vibratome were stained with rabbit anti-TH antibody or rabbit anti-dopamine-glutaraldehyde conjugate (1:500; Millipore). Because glutaraldehyde fixation induces very strong background fluorescence, we performed immunodetection with the avidin-peroxidase complex as described above instead of fluorescence detection.

Western Blotting—To dissect striatal tissues for biochemical assays, we first made a coronal section of 2-mm thickness from approximately +1.5 to 0.5 mm to the bregma using a brain matrix (Neuroscience, Inc., Tokyo). Then the left and right dorsal striata were dissected by a surgical blade under a stereo microscope and homogenized using the Pellet Mixer (TreffLab) in 150 μl of PBS containing 1 mM dithiothreitol, 2 mM EDTA, 2 mM NaF, 1 μg/ml leupeptin, 1 μg/ml pepstatin, 1 mM phenylmethylsulfonyl fluoride, and 0.1 mM pargyline, followed by centrifugation at 20,000 × *g* for 10 min at 4 °C. An aliquot of the supernatant was used for the monoamine assay. In some experiments, ventral midbrain homogenates were prepared similarly, except the positions of coronal sections were approximately −2.5 to −4.5 mm to the bregma. The striatal or ventral midbrain homogenates containing 10 μg of protein were separated by electrophoresis on a 10% SDS-polyacrylamide gel and transferred to a PVDF membrane. The membranes were immunodetected using the following primary antibodies: rabbit anti-TH antibody (1:10,000; Millipore), rabbit anti-AADC antibody (1:20,000) (12), or mouse anti-β-actin antibody (1:10,000; Sigma-Aldrich). Immunoreactive proteins were detected by peroxidase-conjugated secondary antibodies and Immobilon-Western (Millipore). Quantitative analyses were performed with LAS-3000 (Fujifilm).

For better quantification of low level TH proteins by Western blot, we assessed the linearity of the detection using serial dilution of striatal homogenates of the uninjected side (supplemental Fig. 1). Then we employed a range showing a linear relationship between actual loaded proteins (2.5–20 μg, or a 0.125–1.0 ratio) and measured TH protein levels (0.05–1 ratio). Within this range, we made a standard curve and calibrated the TH protein levels accordingly.

For detection of vesicular monoamine transporter 2 (vMAT2) and dopamine transporter (DAT) proteins, a crude synaptosomal fraction was prepared by homogenizing striatal tissues in 4 mM HEPES buffer containing 0.32 M sucrose, 2 mM NaF, 1 μg/ml leupeptin, 1 μg/ml pepstatin, 1 mM phenylmethylsulfonyl fluoride, and 0.1 mM pargyline. The homogenate was centrifuged at 900 × *g*, the supernatant was further centrifuged at 14,500 × *g*, and the resulting pellet (P2 fraction) was dissolved in 80 μl of the same HEPES buffer containing 1% SDS. Protein concentration was determined by the DC protein assay (Bio-Rad). 20 μg of each protein sample was analyzed by Western blot using the following primary antibodies: rabbit anti-vMAT2 antiserum (1:500; Synaptic Systems), rabbit anti-DAT antibody (1:500; Millipore), rabbit anti-TH antibody (1:10,000; Millipore), or mouse anti-β-actin antibody (1:10,000; Sigma-Aldrich).

For the detection of phospho-TH proteins, striatal homogenates were prepared by immediate boiling of a whole brain for 5 min after dissection, followed by isolation of striata and homogenization and sonication in 0.1 M Tris-HCl (pH 6.8) buffer containing 1% SDS. Protein concentration was determined by the DC protein assay (Bio-Rad). 60 μg of each protein sample was analyzed by Western blot using the following primary antibodies: rabbit anti-Ser(P)-40-TH antibody (1:2,000; Millipore), rabbit anti-p31-TH antibody (1:2,000; Millipore), or rabbit anti-TH antibody (1:10,000; Millipore).

Monoamine Assay—Aliquots of striatal supernatant were deproteinized by 60 mM perchloric acid with 30 μM EDTA and 30 μM pargyline on ice for 30 min and centrifuged at 20,000 × *g* for 15 min. The monoamine levels in the supernatant were analyzed by high performance liquid chromatography (HPLC) with an SC5-ODS column (EICOM) and a mobile phase buffer containing 84 mM acetic acid-citrate (pH 3.5), 5 μg/ml EDTA, 190 mg/ml sodium 1-octane sulfonate, and 16% methanol. Monoamines were detected by electrochemical detection (ECD-100, EICOM).

Biopterin contents were measured as described previously (43). Briefly, the deproteinized homogenates were oxidized by 0.1 M HCl containing 0.1% I_2 and 0.2% KI for 1 h at room temperature, followed by centrifugation at 20,000 × *g* for 10 min. The supernatants were neutralized by 0.2% ascorbic acid and then subjected to HPLC analyses with Inertsil ODS-3 column (GL Sciences) and a mobile phase buffer containing 10 mM

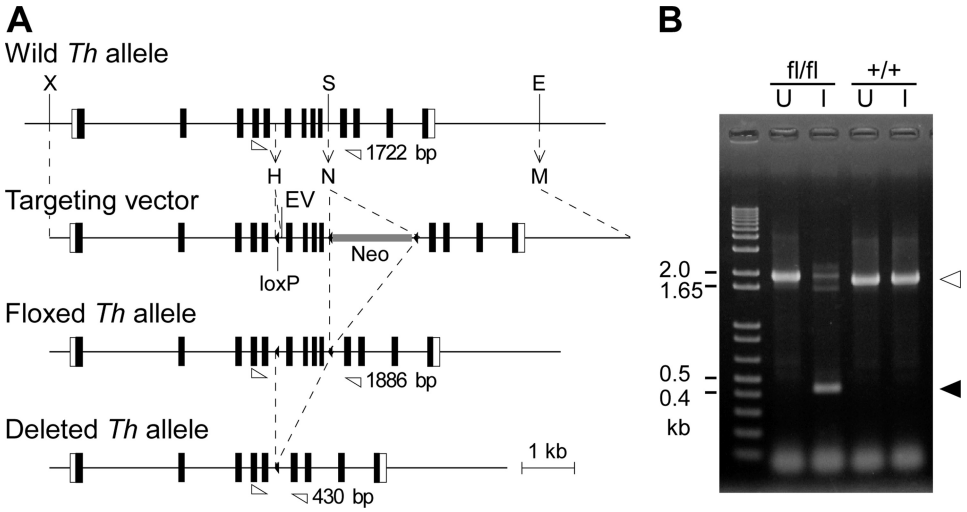

FIGURE 1. **Ablation of the *Th* gene by AAV-Cre injection into the SNc of the floxed *Th* mice.** *A*, schematic representation of the targeting vector for the generation of the floxed *Th* allele. *E*, EcoRI; *H*, HindIII; *M*, MluI; *N*, NotI; *S*, SpeI; *X*, XhoI; *Neo*, neomycin-resistant cassette. *Broken arrows* represent the generation or replacement of a restriction site. Exons are represented by *boxes*. The positions of the primers designed for the detection of genomic DNA recombination by PCR are indicated by *open triangles* with resulting PCR product sizes. *B*, PCR detection of genomic DNA recombination using primers for wild type (*open arrowhead*) or deleted *Th* (*closed arrowhead*) alleles. The template genomic DNA was prepared from the uninjected (*U*) or injected (*I*) side of the of the $Th^{fl/fl}$ or $Th^{+/+}$ mice 2 weeks after the unilateral microinjection of the AAV-Cre into the SNc. Note that the *Th* gene recombination was detected only in the injected side of the SNc of the $Th^{fl/fl}$ mice but not in the uninjected side of the $Th^{fl/fl}$ mice and the $Th^{+/+}$ mice.

$NaPO_4$ (pH 6.9) and a fluorescence detector (excitation 350 nm/emission 440 nm; RF-10A, Shimadzu, Tokyo).

Estimation of in Vivo L-DOPA Synthesis Activity per TH Protein Level—*In vivo* L-DOPA synthesis activity was evaluated by measuring the L-DOPA levels that accumulated in 30 min after the administration of 3-hydroxybenzylhydrazine dihydrochloride (NSD-1015, Sigma-Aldrich), an AADC inhibitor, to mice (100 mg/kg, intraperitoneal). The striatal tissues were homogenized using a pellet mixer (TreffLab) in 150 μl of PBS containing 1 mM dithiothreitol, 2 mM EDTA, 2 mM NaF, 1 μg/ml leupeptin, 1 μg/ml pepstatin, 1 mM phenylmethylsulfonyl fluoride, and 0.1 mM pargyline, followed by centrifugation at 20,000 $\times$ *g* for 10 min at 4 °C. An aliquot of the supernatant was used for assaying protein concentration by Bradford method, and Western blot to assess the TH protein levels. Another aliquot was deproteinized by 60 mM perchloric acid with 30 μM EDTA and 30 μM pargyline on ice for 30 min and centrifuged at 20,000 $\times$ *g* for 15 min. The supernatant was neutralized by K_2CO_3, and L-DOPA was purified by Al_2O_3 powder. The L-DOPA level was analyzed by HPLC with a NUCLEOSIL 100-7C18 reverse-phase column with a mobile phase buffer containing 0.1 M $NaPO_4$ (pH 3.5), 8 μM EDTA and electrochemical detection. To evaluate the *in vivo* L-DOPA synthesis activity per TH protein, L-DOPA accumulation was normalized to TH protein levels estimated by Western blot.

Rotation Test—Mice were placed in a round bowl (25 cm in diameter) for 20 min for acclimation. The mice were administered with 1-[2-[bis-(4-fluorophenyl)methoxy]ethyl]-4-(3-phenylpropyl)piperazine dihydrochloride (GBR12909; Tocris Bioscience; intraperitoneal, 30 mg/kg) and returned to the same bowl, and the behavior was videorecorded. The rotations were counted by visual observation for a 60-min period immediately after intraperitoneal injection. One rotation was defined by the animal completing a 360° turning without turning back in the opposite direction.

Statistics—The Mann-Whitney *U* test, Wilcoxon's signed rank test, or Steel's test was used as required. Spearman's rank correlation was used to evaluate a correlation between two groups. p values of <0.05 were considered significant. The data are shown as individual data points and mean values or as mean $\pm$ S.E., as indicated. Exponential and liner fittings were performed with Igor Pro 6.2 (WaveMetrics).

RESULTS

Production of Floxed Th Mice and Th Gene Ablation by AAV-Cre—First, we generated the floxed *Th* mice ($Th^{fl/fl}$) in which exons 6–9 of the *Th* gene were flanked by *loxP* sites (Fig. 1*A*). We used AAV-Cre to induce DNA recombination *in vivo* by performing a unilateral stereotaxic microinjection of the virus into the SNc of the adult floxed *Th* mice. Microinjection of AAV-Cre into the SNc induced DNA recombination in 2 weeks when we examined the substantia nigra tissue samples by PCR (Fig. 1*B*). *Th* gene recombination was detected in the injected side SNc of the $Th^{fl/fl}$ mice but not in the uninjected side of the $Th^{fl/fl}$ mice and both sides of the $Th^{+/+}$ mice. Thus, the floxed *Th* mice and AAV-Cre enabled us to induce *Th* gene ablation in the adult mouse midbrain.

Abrogation of TH Protein Expression in SNc Dopaminergic Neurons—Using immunohistochemistry, we next examined the effect of the AAV-Cre injection on TH protein expression in the SNc. The TH protein immunoreactivity was absent in the majority of neurons in the SNc 2 weeks after the AAV-Cre injection (Fig. 2*A* and *B*). We found that the number of TH-positive dopaminergic neurons normalized to the uninjected side was reduced by as early as 2 weeks, with the mean ratios of 38, 30, and 40% at 2, 4, and 8 weeks after the AAV-Cre injection, respectively, whereas they were unchanged in the $Th^{+/+}$ mice (97% at 8 weeks; Steel's test, $p = 0.0239$, 0.0166, and 0.0061 for the $Th^{fl/fl}$ mice at 2, 4, and 8 weeks, respectively, compared with the $Th^{+/+}$ at 8 weeks; Fig. 2*C*).

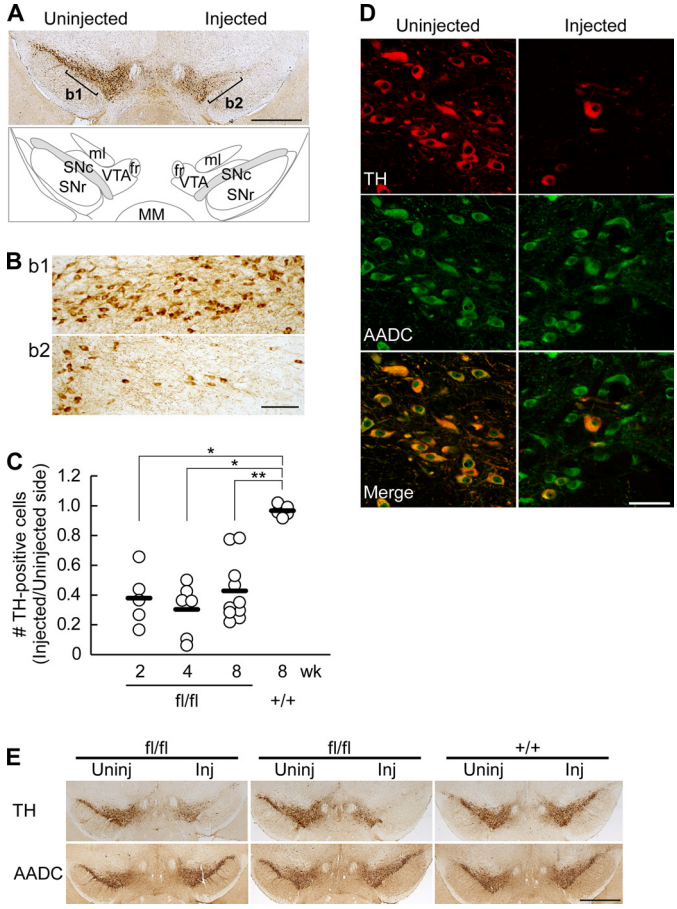

FIGURE 2. **AAV-Cre-induced loss of TH expression in the SNc.** *A*, a representative image of a midbrain slice immunostained for TH (*top*) and a schematic atlas (*bottom*). Serial coronal sections of the midbrains of the $Th^{fl/fl}$ mice were prepared 8 weeks after the AAV-Cre injection and were immunostained for TH. The SNc in the atlas is indicated by the *hatched area*. *fr*, fasciculus retroflexus; *ml*, medial lemniscus; *MM*, medial mammillary nucleus; *SNr*, substantia nigra pars reticulata; *VTA*, ventral tegmental area. *B*, magnified views of the uninjected side (*b1*) and injected side (*b2*) SNc as indicated in *A*. *C*, summary of the ratio of TH-positive cell numbers in the injected side SNc to the uninjected side. *Open circles* indicate the values from individual animals, and *bars* indicate the means. $n = 5$, 6, 11, and 5 brains for 2, 4, and 8 weeks ($Th^{fl/fl}$ mice) and 8 weeks ($Th^{+/+}$ mice) after injection, respectively. *, $p < 0.05$; **, $p < 0.01$, Steel's test. *D*, immunofluorescence staining for TH (*red*) and AADC (*green*) of the SNc of the $Th^{fl/fl}$ mice examined 2 weeks after the injection of AAV-GFP/Cre. TH and AADC were visualized with Alexa546 and Alexa633, respectively, distinguishing from GFP signal, and *pseudocolored* confocal images are shown. Note that the number of TH-expressing neurons was clearly reduced in the AAV-GFP/Cre-injected side, whereas the AADC, another dopaminergic neuron marker, remained expressed. *E*, TH deletion induces no apparent cell death in 16 weeks. Midbrain slices from two $Th^{fl/fl}$ mice and one $Th^{+/+}$ mouse were immunostained for TH and AADC 16 weeks after the AAV-Cre microinjection. Whereas the TH-expressing neurons were reduced in the injected side of the SNc of the $Th^{fl/fl}$ mice, the number of AADC-expressing neurons was apparently unaffected, suggesting that the dopaminergic neurons do not show cell death in the absence of TH in 16 weeks. *Scale bars*, 1 mm (*A*), 100 μm (*B*), 50 μm (*D*), and 1 mm (*E*).

To confirm a selective loss of TH protein, we also performed double immunofluorescence histochemistry for TH and aromatic AADC, a dopaminergic neuron marker. We used AAV-GFP/Cre for the purpose of labeling infected cells, but GFP expression in these neurons was too weak for detection, so we immunostained TH and AADC with Alexa546 and Alexa633 fluorophores, respectively, distinguishing from GFP signals. We found that the AADC immunoreactivity was preserved in the TH-negative neurons in the SNc 2 weeks after the AAV-GFP/Cre injection (Fig. 2*D*), suggesting that the AAV-GFP/Cre injection induced an efficient *Th* gene ablation without inducing cell death or damage. Moreover, AADC expression in the SNc was apparently unaffected in the $Th^{fl/fl}$ mice up to 16 weeks following the AAV-Cre injection, when the majority of the SNc dopaminergic neurons lost TH expression (Fig. 2*E*). These data suggest that dopamine is not essential for the survival of dopaminergic neurons in adult brains.

Slower Reduction of TH Proteins in Axon Terminals of Nigrostriatal Projection—The dopaminergic neurons in the SNc project their axons toward the striatum and form dense synapses (23, 24), where abundant TH proteins were contained. We quantitatively examined the reduction of the TH protein in the striatum by Western blot (Fig. 3*A* and *B*). The TH protein level was gradually reduced in the AAV-Cre injected side compared with the uninjected side in $Th^{fl/fl}$ mice, to 75, 50, and 39% at 2, 4, and 8 weeks after the AAV-Cre injection, respectively, whereas the levels were unchanged in the $Th^{+/+}$ mice (104% at 8 weeks; Steel's test, $p = 0.0932$, 0.0071, and 0.0059 for the $Th^{fl/fl}$ mice at 2, 4, and 8 weeks, respectively, compared with the $Th^{+/+}$ at 8 weeks; Fig. 3*B*). AADC protein levels did not show significant changes (Steel's test, $p = 0.77$, 0.92, and 0.88 for the $Th^{fl/fl}$ mice at 2, 4, and 8 weeks, respectively, compared with the $Th^{+/+}$ at 8 weeks; supplemental Fig. 2*A*).

We noticed that the reduction of TH protein level in the striatum could be slower than the reduction of the number of TH-expressing cells in the SNc because the difference between the two seemed remarkable at 2 weeks. To further investigate the difference, we compared the TH protein reductions in the striatum with that in ventral midbrain tissue, including SNc, using Western blot (Fig. 3*C*). We found that the TH protein reduction in the striatum showed a delay by about 2 weeks, whereas the decay time constants were similar ($\tau = 2.06$ and 2.04 weeks for the ventral midbrain and striatum, respectively).

We also used immunofluorescence histochemistry to examine the expression of TH and AADC in the striatum (Fig. 3*D*). Two weeks after the AAV-Cre injection, the number of TH-expressing axons in the injected side of the striatum of the $Th^{fl/fl}$ mice was only slightly reduced compared with the uninjected side, which was consistent with the Western blot data. However, the number of TH-expressing axons was decreased profoundly 8 weeks after the AAV-Cre injection. The number of AADC-expressing axons was apparently unchanged, suggesting that the axon terminals of the dopaminergic neurons remained mostly intact. These Western blot and immunohistochemical data indicate differential regulation of TH protein levels between axon terminals (striatum) and soma (SNc). Also, the *Th* gene ablation led to an almost complete and selective loss of TH protein in a subset of dopaminergic axons.

Better Maintenance of Striatal Dopamine Levels than TH Protein Levels—To investigate if dopamine levels follow the reduction of TH protein levels in the striatum, we assayed striatal monoamine contents using the same striatal extracts used in the Western blot analysis (Fig. 4*A*). The dopamine contents decreased gradually to around 98, 79, and 69% at 2, 4, and 8 weeks after the AAV-Cre injection, respectively, in the $Th^{fl/fl}$ mice but not in the $Th^{+/+}$ mice (104% at 8 weeks; Steel's test, $p = 0.98$, 0.0475, and 0.0637 for 2, 4, and 8 weeks in the $Th^{fl/fl}$

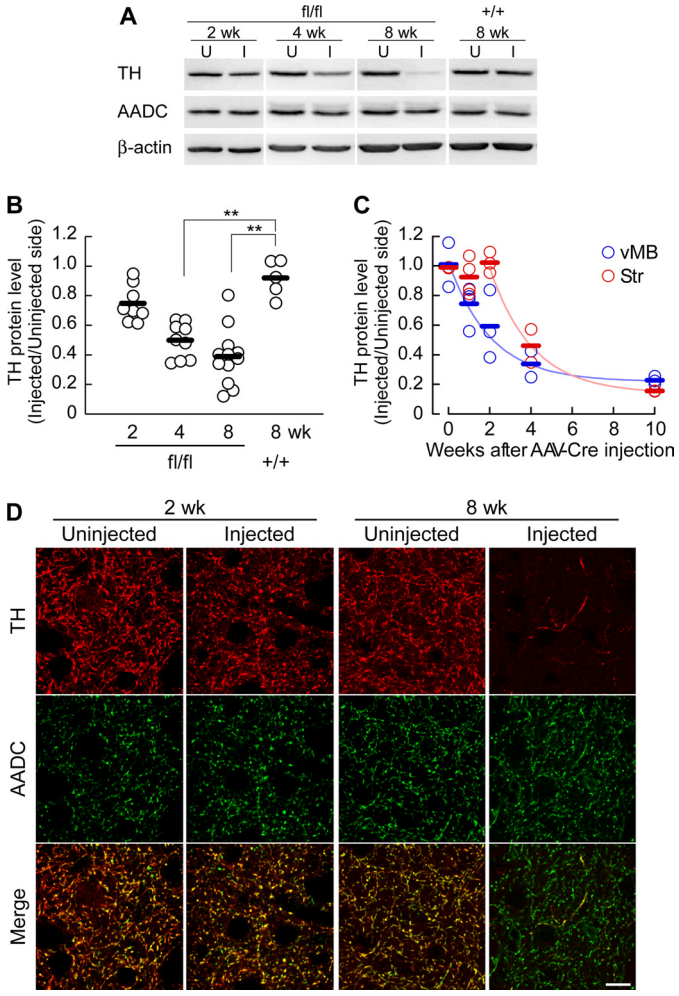

FIGURE 3. **Decrease in striatal TH protein levels after *Th* gene ablation.** *A*, striatal homogenates of each genotype were prepared 2, 4, or 8 weeks after the unilateral AAV-Cre injection into the SNc, and Western blot analysis was performed with antibodies against TH, AADC, and β-actin. *U* and *I*, uninjected and injected sides of the striatum, respectively. *B*, summarized quantitative analyses of Western blots for the striatal TH protein levels. The ratios of the protein level of the injected side to the uninjected side are plotted on the *vertical axis*. The *open circles* indicate the values from individual animals, and the *bars* indicate the means. $n = 8$, 9, 12, and 5 brains for 2, 4, and 8 weeks ($Th^{fl/fl}$ mice) and 8 weeks ($Th^{+/+}$ mice) after injection, respectively. *, $p < 0.05$; **, $p < 0.01$, Steel's test. *C*, comparison of TH protein levels in the striatum and ventral midbrain by Western blot. Tissue homogenates were prepared from the injected side and uninjected side of the ventral midbrain (*vMB*) and striatum (*Str*) of $Th^{fl/fl}$ mice and were subjected to Western blots for TH. $n = 2$, 4, 3, 2, and 3 for 0, 1, 2, 4, and 10 weeks after AAV-Cre injection, respectively. Data were fitted with an *exponential curve*. For the striatum, fitting was performed from 2 weeks because there was no apparent reduction before 2 weeks in this data set. *D*, decrease in the number of TH-expressing axons in the striatum. Striatal slices of the $Th^{fl/fl}$ mice were prepared 2 and 8 weeks after the injection of AAV-GFP/Cre and were immunohistochemically stained for TH (*red*) and AADC (*green*). TH and AADC were visualized as in Fig. 2*D*. *Merged images* are shown at the *bottom*. Images from the uninjected and injected side of the striatum are shown as indicated. *Scale bar*, 10 μm.

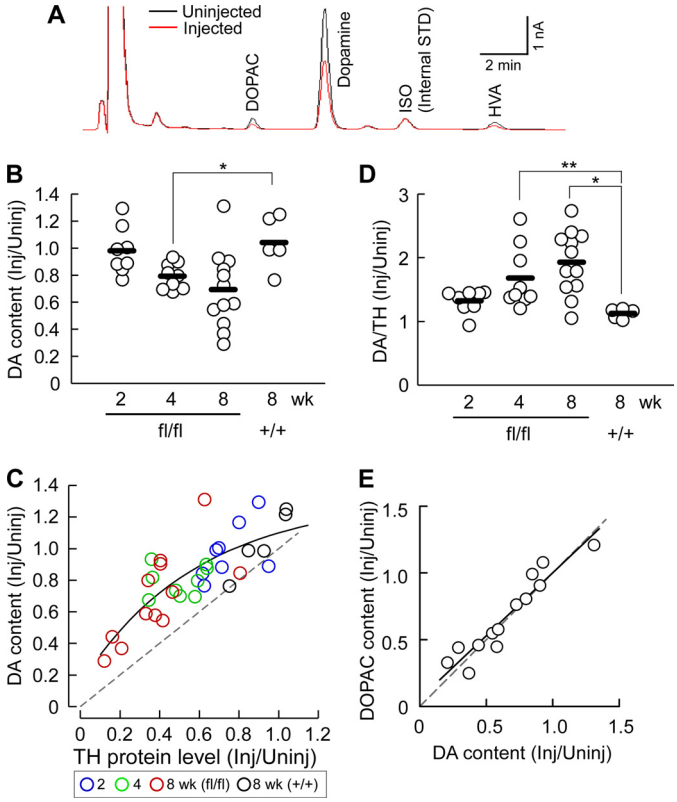

FIGURE 4. **The tissue dopamine contents are better maintained than TH protein levels in the striatum.** *A*, representative chromatograms of the monoamine assay with the homogenates from the uninjected and injected side striata from a $Th^{fl/fl}$ mouse 8 weeks after the injection of AAV-Cre. *B*, summarized DA contents in the striatum after the unilateral AAV-Cre injection to the SNc in the $Th^{fl/fl}$ and $Th^{+/+}$ mice. The monoamine assays were performed using the same extracts used in Fig. 3. The ratios of the dopamine contents in the injected side to the uninjected side are shown. The *open circles* indicate the values from individual animals, and the *bars* indicate the means. $n = 8$, 9, 12, and 5 brains for 2, 4, and 8 weeks ($Th^{fl/fl}$ mice) and 8 weeks ($Th^{+/+}$ mice) after the injection, respectively. *, $p < 0.05$, Steel's test. The mean dopamine contents in the uninjected side striata were 147.2 ± 10.2 and 158.1 ± 6.7 pmol/mg protein for $Th^{fl/fl}$ and $Th^{+/+}$ mice, respectively at 8 weeks (Steel's test, $p = 0.86$). *C*, the relationship between dopamine contents and TH protein levels. The *circles* represent data from individual animals and are *color-coded* by weeks after the AAV-Cre injection as indicated. The *dotted line* has a slope of 1. The *solid line* indicates an exponential curve fitting. The *points above* the *dotted line* suggest a higher dopamine level per TH protein level in the injected side compared with the uninjected side. *D*, ratio of the dopamine content to the TH protein level normalized to the uninjected side. $n = 8$, 9, 12, and 5 brains for 2, 4, and 8 weeks ($Th^{fl/fl}$ mice) and 8 weeks ($Th^{+/+}$ mice) after the injection, respectively. We excluded one outlier that showed very low TH protein levels and a high DA/TH ratio (29.8) from the 8-week $Th^{fl/fl}$ group. *, $p < 0.05$; **, $p < 0.01$, Steel's test. *E*, the relationship between DOPAC and dopamine contents in the $Th^{fl/fl}$ mice 8 weeks after the AAV-Cre injection. The data indicate the ratio of the DOPAC contents in the AAV-Cre-injected side of the striatum normalized to the uninjected side. The *open circles* indicate individual data. The *dotted line* has a slope of 1, and the *solid line* indicates a linear fitting. $n = 13$ mice. Spearman's rank correlation, $p < 0.0001$, $\rho = 0.96$ for DOPAC *versus* dopamine.

mice, respectively, compared with the $Th^{+/+}$ mice at 8 weeks; Fig. 4*B*). Notably, these reductions of dopamine contents were not as striking as those of TH protein levels (Fig. 2*C*). To evaluate the relationship between dopamine and TH, we plotted dopamine contents against TH protein levels (Fig. 4*C*). We found that dopamine contents were less affected than the TH protein levels, and the relationship was fitted well with an exponential curve ($\chi^2 = 0.7391$). The dopamine contents did not show a remarkable reduction until the TH protein levels were decreased by around 50%. Accordingly, the ratios of dopamine contents to TH protein levels were increased, with ratios of 1.32, 1.68, and 1.93 at 2, 4, and 8 weeks after the AAV-Cre injection, respectively, in the $Th^{fl/fl}$ mice, whereas it remained 1.1 in the $Th^{+/+}$ mice at 8 weeks (Steel's test, $p = 0.0665$, 0.0071, and 0.0157 for 2, 4, and 8 weeks for the $Th^{fl/fl}$ mice, respectively, compared with the $Th^{+/+}$ mice at 8 weeks; Fig. 4*D*).

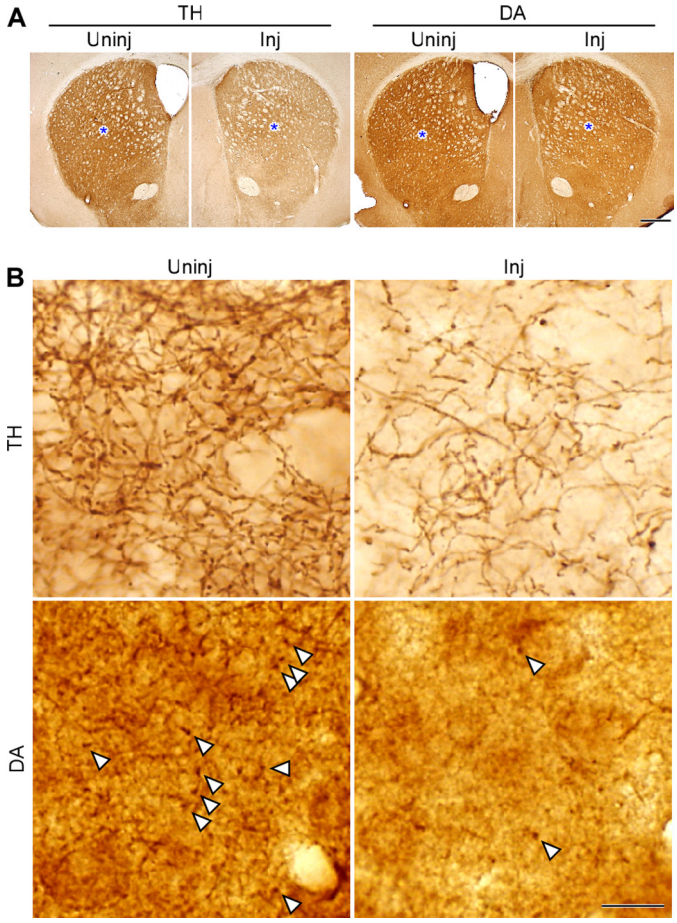

FIGURE 5. **TH and dopamine distribution in the striatum.** *A*, immunohistochemical detection of the striatal TH and DA in the striatum of the $Th^{fl/fl}$ mouse. The mice were fixed with glutaraldehyde 8 weeks after the injection of AAV-GFP/Cre, and the slices cut with a vibratome were stained with antibodies against TH or dopamine. Note that the TH signal in the injected side (*Inj*) was decreased compared with the uninjected side (*Uninj*), whereas the DA signal was less affected. *B*, magnification images of the regions indicated by *asterisks* in *A*, showing TH-expressing axon fibers and dopamine-containing axonal boutons. *Arrowheads* indicate representative puncta of the dopamine signals. *Scale bars*, 0.5 mm (*A*) and 10 μm (*B*).

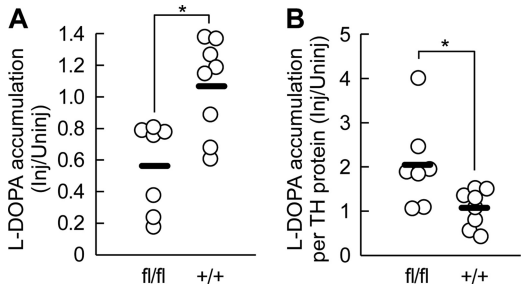

FIGURE 6. **Enhanced *in vivo* L-DOPA synthesis activity per TH protein level.** L-DOPA synthesis activities per TH protein level were estimated by measuring L-DOPA accumulation after *in vivo* administration of NSD-1015, an AADC inhibitor. Striatal homogenates were prepared 30 min after NSD-1015 administration (100 mg/kg, intraperitoneally). L-DOPA levels were measured by HPLC, and TH protein levels were assayed by Western blot. The mice were examined 8 weeks after the AAV-Cre injection. *A*, summary of L-DOPA accumulation in $Th^{fl/fl}$ and $Th^{+/+}$ mice. Data are shown as L-DOPA level in the injected side normalized by the uninjected side. The *open circles* indicate the values from individual animals, and the *bars* indicate the means. The mean L-DOPA level in the uninjected side of the $Th^{+/+}$ mice was 42.1 $\pm$ 7.3 pmol/mg protein. *B*, summary of L-DOPA accumulation normalized to the TH protein levels examined by Western blot, providing apparent L-DOPA synthesis activity per TH protein level. *, $p < 0.05$, Mann-Whitney *U* test.

It is known that unilateral depletion of dopamine in the rodent nigra induces ipsilateral rotation behavior in response to reagents enhancing dopaminergic transmission (25, 26). Consistently, $Th^{fl/fl}$ mice with severe unilateral dopamine depletion showed ipsilateral rotation behavior when administered with GBR12909, a potent DAT inhibitor (supplemental Fig. 2*B*), demonstrating the validity of our genetic manipulation to disrupt nigrostriatal dopaminergic transmission.

To further examine the tissue level alterations in the dopamine distribution, we used immunohistochemistry to determine the expression pattern for dopamine and TH in the striatum 8 weeks after the AAV-Cre injection. The mice were fixed transcardially with glutaraldehyde, and the striatal slices were stained with an antibody raised against dopamine-glutaraldehyde conjugate. We used immunoenzyme detection instead of immunofluorescence detection, because glutaraldehyde fixation causes a high fluorescence background. At a lower magnification, TH immunoreactivity was clearly reduced in the AAV-Cre-injected side of the $Th^{fl/fl}$ mice, whereas the dopamine immunoreactivity was only moderately reduced (Fig. 5*A*). These data are consistent with Western blot and monoamine assay results. Higher magnification views showed a reduction in the number of TH-expressing axon fibers in the AAV-Cre-injected side of the $Th^{fl/fl}$ mice (Fig. 5*B*) as observed by immunofluorescence staining (Fig. 3*D*). Moreover, the number of punctate signals of dopamine was also greatly decreased (Fig. 5*B*), suggesting that dopamine levels in the TH-lost axons were substantially reduced. Collectively, these data indicate a compensatory regulation of dopamine levels for a decrease in the TH protein levels. Because TH expression remained in only a subset of dopaminergic axons, these data raise the possibility that a decrease in dopamine synthesis induces a compensatory up-regulation of dopamine synthesis and/or storage in other axons.

Mechanisms of Dopamine Maintenance against TH Protein Loss—The homeostatic compensation of dopamine levels may accompany either an increase in the synthesis of dopamine or a decrease in the degradation of dopamine. To examine the degradation rate of dopamine, we measured the contents of 3,4-dihydroxyphenylacetic acid (DOPAC) and homovanillic acid (HVA), the two major metabolites of dopamine. Reductions of DOPAC and HVA contents were well correlated with that of dopamine in the $Th^{fl/fl}$ mice (Fig. 4*E*). Comparison between injected and uninjected sides showed no difference in the ratio of DOPAC to dopamine (DA) (injected side, 0.12 $\pm$ 0.02; uninjected side, 0.15 $\pm$ 0.03; Wilcoxon's signed rank test, $p = 0.16$) and in the ratio of HVA to dopamine (injected side, 0.13 $\pm$ 0.01; uninjected side, 0.14 $\pm$ 0.01; Wilcoxon's signed rank test, $p = 0.43$; supplemental Fig. 3). These data suggest that the degradation rate of dopamine was not significantly changed.

To explore a possible change in the activity of dopamine synthesis pathway, we evaluated *in vivo* L-DOPA synthesis activity by measuring L-DOPA accumulation 30 min after administration of NSD-1015, an AADC inhibitor, 8 weeks after the AAV-Cre injection. We found that the L-DOPA accumulation in the injected side of the striatum was significantly lower in the $Th^{fl/fl}$ mice compared with the $Th^{+/+}$ mice (Mann-Whitney *U* test, $p = 0.0206$; Fig. 6*A*). We then estimated the apparent L-DOPA

synthesis activity per TH protein by normalizing the L-DOPA accumulation with TH protein levels estimated by Western blot analysis. We found that the L-DOPA accumulation per TH protein in the injected side striatum was significantly higher in the $Th^{fl/fl}$ mice than in the $Th^{+/+}$ mice (Mann-Whitney *U* test, $p = 0.0279$; Fig. 6*B*). Considering that L-DOPA is mostly synthesized by TH (14), and the TH proteins remained to be expressed in only a subset of axons, these data suggest that dopamine synthesis activity in the remaining TH-positive axons was augmented to compensate for dopamine level.

Further, we examined if TH phosphorylation at Ser-31 and Ser-40 (27), the two major phosphorylation sites for TH activation, was elevated. However, we did not find a significant change in the phosphorylation states of these Ser residues by Western blot (supplemental Fig. 4). We also measured the contents of biopterin, an essential cofactor for TH, but the contents were not significantly different between the injected and uninjected side (uninjected side, 6.72 ± 0.54 pmol/mg protein; injected side, 6.64 ± 0.49 pmol/mg protein; Mann Whitney *U* test, $p = 0.95$). Thus, the long term up-regulation of L-DOPA synthesis activity may be supported by other molecular mechanisms (*e.g.* a relief of the feedback inhibition of TH by dopamine as a consequence of impaired dopamine synthesis).

In axon terminals, synthesized dopamine is primarily stored in synaptic vesicles, and released dopamine is partly recycled by DAT. When the number of TH-expressing axons was greatly reduced, the manner of dopamine storage could be changed for adaptation. In this context, we examined the level of two major dopamine transporters: vMAT2 and DAT. Western blot analysis showed no significant change in the vMAT2 and DAT protein levels in the injected side striatum compared with the uninjected side in the $Th^{fl/fl}$ mice, despite the great reduction of TH protein levels (supplemental Fig. 5). These data suggest that the numbers of dopaminergic synaptic vesicles and terminals were not grossly altered. Instead, because the majority of dopaminergic axons do not contain normal level of dopamine (Fig. 5*B*), despite the moderate decrease in tissue dopamine contents (Fig. 4), the vesicular dopamine contents in the TH-expressing axons may be increased, and/or TH-negative axons may uptake and contain low level dopamine.

DISCUSSION

Selective Loss of TH Protein in a Subset of Dopaminergic Neurons without Neuronal Degeneration—We took advantage of the Cre-*loxP* system in mice, which enabled us to selectively ablate the *Th* gene and block dopamine synthesis in adult brains. TH expression in the SNc was lost in a subset of SNc dopaminergic neurons by as early as 2 weeks after the AAV-Cre injection. The TH protein level and the number of TH-expressing axons in the striatum were clearly reduced 8 weeks after the AAV-Cre injection. Severe dopamine deficiency accompanied ipsilateral rotation behavior when stimulated with the DAT inhibitor, GBR12909, confirming the integrity of our genetic method to disrupt nigrostriatal dopaminergic transmission.

In contrast, the AADC protein levels and immunohistochemical signals in the striatum and SNc were unaffected 8 or 16 weeks after the AAV-Cre injection. These data suggest that the SNc dopaminergic neurons and axons were mostly preserved for several months without synthesizing dopamine. This is in contrast to neurodegenerative models using neurotoxins, such as 1-methyl-4-phenyl-1,2,3,6-tetrahydropyridine and 6-hydroxydopamine (6-OHDA), which could cause loss of axons and unpredictable side effects. Therefore, our experimental system provides a new animal model of chronic dopamine deficiency in adult brains without neuronal degeneration.

Differential Regulation of TH Protein Level in the Axon Terminals from Soma—Using this *Th* gene ablation strategy in adult brains, we noticed that the decline in the TH protein in the striatum was slower than the reduction of TH-expressing neurons in the SNc (Figs. 2*C* and 3*B*). By direct comparison of TH protein reduction in the striatum and ventral midbrain with Western blotting, we found that the TH protein reduction occurred in a delay, whereas the decay time constants were similar (Fig. 3*C*). This considerable delay of TH protein loss in the striatum suggests a mechanism that maintains the axonal TH protein level for a week or two without *Th* gene transcription. How does such a delay occur?

First, the turnover of TH proteins in axon terminals in the striatum may be slower than that in cell bodies in SNc. In cultured chromaffin cells, the steady-state half-life of the TH protein is about 1 day (28), but it could become longer than 10 days by treatment with translational inhibitors (29). Moreover, incubation with transcriptional inhibitors for 3 days caused no significant loss of the TH protein, although 90% of the TH mRNA was lost (29). Axonal translation may be involved for such a prolonged delay of protein degradation (30, 31). Thus, the difference in TH protein turnover in axon terminals and cell bodies located in SNc may be supported by those multiple regulatory mechanisms.

In addition, the delayed reduction of TH proteins may be attributable to slow axonal transport of TH proteins from soma to axons. Although the mechanism underlying axonal TH transport is not fully understood, the projection from SNc to the striatum in mice is about 2–10 mm, depending on axonal branching (22, 23). The axonal transport of TH was reported to be about 2 mm/h in chicken sciatic nerves (32), but it could be different in the brain because the cytosolic proteins are delivered by the slow axonal transport system at 0.1–8 mm/day (33, 34). These reports raise a possibility that it takes a week or more to transport TH proteins from a soma to axon terminals in the mouse nigrostriatal projection.

Regulation of Dopamine Levels by TH Protein Level and Activity in the Striatum—By quantitative comparison of dopamine contents with TH protein levels in the same striatal tissues, we found that dopamine contents were not simply determined by the TH protein level only. Notably, even 50% loss of TH protein did not remarkably change the dopamine contents. Eight weeks after the AAV-Cre injection, the TH protein levels were reduced to 39%, on average, whereas the dopamine contents were reduced to 69%. Immunohistochemical data showed a similar trend of difference. This finding is consistent with a previous report that dopamine contents in the brain of the adult $Th^{+/-}$ heterozygous mice are normally maintained despite a significant decrease in TH activity (12). Thus, these data indicate that the dopamine levels were primarily determined by TH

protein level but also influenced by another mechanism in the nigrostriatal projection.

In this study, we showed that (i) the TH protein expression was abrogated in a subset of dopaminergic neurons (AAV-Cre-infected neurons); (ii) the striatal dopamine contents were better maintained than the TH protein levels; and (iii) *in vivo* L-DOPA synthesis activity per TH protein level was enhanced. Because L-DOPA synthesis activity was virtually retained in only the TH-expressing axons, these results suggest that L-DOPA synthesis activity per TH protein in a given axon is partly affected by dopamine synthesis in the neighboring axons. Such trans-axonal regulation of dopamine synthesis activity might be a basis for the homeostasis of dopaminergic transmission in the striatum.

Consistent with our data, in a rat model of preclinical parkinsonism where nigrostriatal dopaminergic neurons were lesioned by 6-OHDA, TH activity was increased relative to dopamine loss (35). In such models generated with 6-OHDA, however, it is difficult to know if the enhanced TH activity observed after 6-OHDA administration is a result of a direct toxic effect of 6-OHDA on the remaining axons, a cell death of neighboring axons, or a decrease in tissue dopamine level. In contrast, our genetic manipulation specifically targets the *Th* gene in AAV-Cre-infected neurons, so our results demonstrate the effect of *Th* gene deletion on TH protein levels, dopamine contents, and L-DOPA synthesis activity more clearly and simply.

It remains to be determined how trans-axonal compensation of dopamine is mediated. For example, TH homospecific activity may be changed for the compensation by phosphorylation. D2 autoreceptors on dopaminergic axon terminals may be involved in controlling the dopamine level (36). However, it is not clear whether D2 autoreceptors modify dopamine synthesis in the long term. For example, chronic administration of haloperidol, a D2 receptor inhibitor, does not increase the basal levels of Ser(P)-31-TH and Ser(P)-40-TH in mice (37). We could not detect significant change in the Ser(P)-31-TH and Ser(P)-40-TH levels.

TH is also controlled by a feedback inhibition loop by dopamine (27). For example, a decrease in extracellular dopamine level by *Th* gene ablation may cause lower dopamine reuptake (38), lower local dopamine concentration in axon terminals, and a relief of TH from the feedback inhibition. Previous reports suggest that the concentration of released dopamine can be on the order of micromolar and is quickly taken up by DAT into dopaminergic axons (38). Because intracellular dopamine concentration is probably <100 nM (39), local intracellular dopamine concentration could be affected by dopamine reuptake. Meanwhile, TH has two dopamine-binding sites: high affinity ($K_d < 4$ nM) and low affinity ($K_d = 90$ nM) (40). Therefore, most TH proteins would be the dopamine-bound form for the high affinity site, whereas the low affinity site may be more relevant to feedback inhibition by dopamine (40).

Alternatively, there is a circuit level feedback (8) or neurotrophic factors, such as glial cell-derived neurotrophic factor (41). Further studies will be required to clarify the signaling mechanisms underlying the trans-axonal regulation of dopamine levels.

We found that the ratio of DOPAC and HVA contents to dopamine did not change, whereas, in Parkinson disease patients and model animals, DOPAC/DA and HVA/DA ratios were reported to be increased (7, 10, 42). This difference may exist because in our experimental conditions, most of the dopaminergic axons were preserved after the *Th* gene ablation, and those axons may have participated in the reuptake of extracellular dopamine, resulting in minimal effects on the dopamine degradation rate.

Adjusting Dopamine Storage for Compensation—If the number of dopamine-synthesizing axons was decreased by more than half, where and how were dopamine molecules stored for compensation? Because we did not observe any gross changes in the vMAT2 and DAT protein levels, it is unlikely that the numbers of dopaminergic synaptic vesicles and terminals were drastically changed. Otherwise, vesicular dopamine contents may be increased in the remaining TH-expressing axons for the compensation. For example, treatment of cultured dopaminergic neurons with L-DOPA or glial cell-derived neurotrophic factor increased vesicular dopamine levels more than 3-fold (41). Alternatively, it is also possible that the low level dopamine was contained in the TH-negative axons through the reuptake of spilled-over dopamine from neighboring synapses. This mechanism is consistent with the idea that released dopamine is spilled over and taken up by neighboring axons (38). Thus, the compensation of dopamine levels in our experimental system may accompany an increase in vesicular dopamine contents and/or spill-over and reuptake of released dopamine by TH-negative axons.

Taken together, in this study, we develop a conditional gene targeting method to efficiently and selectively inactivate the *Th* gene in the SNc dopaminergic neurons in adult mice without inducing neuronal degeneration. The analysis of these mutant mice revealed that TH protein levels in the axon terminals are regulated differently from the level in the soma, and the tissue dopamine levels are under trans-axonal compensatory regulation, where the reduction of dopamine in some axons induces up-regulation of dopamine synthesis activity in other axons. We believe that the present findings represent at least one of the compensatory mechanisms in Parkinson disease and are related to actions of remedies for psychiatric disorders.

Acknowledgments—We are most grateful to Professor Pierre Chambon for supporting this project. We thank Jean-Marc Bornert and the Institut de Génétique et de Biologie Moléculaire et Cellulaire/Institut Clinique de la Souris embryonic stem and mouse facility for excellent technical assistance. We thank Naomi Takino and Hiroko Nishida for technical assistance in constructing the AAV vectors. We thank Felix Schlegel for technical assistance with immunohistochemistry. We thank Dr. Pavel Osten for kindly providing the Synapsin I promoter construct.

REFERENCES

1. Graybiel, A. M., Canales, J. J., and Capper-Loup, C. (2000) *Trends Neurosci.* **23,** S71–S77
2. Schultz, W. (2007) *Trends Neurosci.* **30,** 203–210
3. Fahn, S. (2003) *Ann. N.Y. Acad. Sci.* **991,** 1–14
4. Grace, A. A., Floresco, S. B., Goto, Y., and Lodge, D. J. (2007) *Trends*

Neurosci. **30,** 220–227
5. Tye, K. M., Tye, L. D., Cone, J. J., Hekkelman, E. F., Janak, P. H., and Bonci, A. (2010) *Nat. Neurosci.* **13,** 475–481
6. Simpson, E. H., Kellendonk, C., Kandel, E. (2010) *Neuron* **65,** 585–596
7. Bernheimer, H., Birkmayer, W., Hornykiewicz, O., Jellinger, K., Seitelberger, F. (1973) *J. Neurol. Sci.* **20,** 415–455
8. Bezard, E., Gross, C. E., and Brotchie, J. M. (2003) *Trends Neurosci.* **26,** 215–221
9. McCallum, S. E., Parameswaran, N., Perez, X. A., Bao, S., McIntosh, J. M., Grady, S. R., and Quik, M. (2006) *J. Neurochem.* **96,** 960–972
10. Pifl, C., and Hornykiewicz, O. (2006) *Neurochem. Int.* **49,** 519–524
11. Perez, X. A., Parameswaran, N., Huang, L. Z., O'Leary, K. T., and Quik, M. (2008) *J. Neurochem.* **105,** 1861–1872
12. Kobayashi, K., Morita, S., Sawada, H., Mizuguchi, T., Yamada, K., Nagatsu, I., Hata, T., Watanabe, Y., Fujita, K., and Nagatsu, T. (1995) *J. Biol. Chem.* **270,** 27235–27243
13. Thomas, S. A., Matsumoto, A. M., and Palmiter, R. D. (1995) *Nature* **374,** 643–646
14. Zhou, Q. Y., Quaife, C. J., Palmiter, R. D. (1995) *Nature* **374,** 640–643
15. Zhou, Q. Y., and Palmiter, R. D. (1995) *Cell* **83,** 1197–1209
16. Szczypka, M. S., Kwok, K., Brot, M. D., Marck, B. T., Matsumoto, A. M., Donahue, B. A., and Palmiter, R. D. (2001) *Neuron* **30,** 819–828
17. Hnasko, T. S., Perez, F. A., Scouras, A. D., Stoll, E. A., Gale, S. D., Luquet, S., Phillips, P. E, Kremer, E. J., and Palmiter, R. D. (2006) *Proc. Natl. Acad. Sci. U.S.A.* **103,** 8858–8863
18. Nagatsu, T., Levitt, M., and Udenfriend, S. (1964) *J. Biol. Chem.* **239,** 2910–2917
19. Li, X. G., Okada, T., Kodera, M., Nara, Y., Takino, N., Muramatsu, C., Ikeguchi, K., Urano, F., Ichinose, H., Metzger, D., Chambon, P., Nakano, I., Ozawa, K., and Muramatsu, S. (2006) *Mol. Ther.* **13,** 160–166
20. Kadkhodaei, B., Ito, T., Joodmardi, E., Mattsson, B., Rouillard, C., Carta, M., Muramatsu, S., Sumi-Ichinose, C., Nomura, T., Metzger, D., Chambon, P., Lindqvist, E., Larsson, N. G., Olson, L., Björklund, A., Ichinose, H., and Perlmann, T. (2009) *J. Neurosci.* **16,** 15923–15932
21. Dittgen, T., Nimmerjahn, A., Komai, S., Licznerski, P., Waters, J., Margrie, T. W., Helmchen, F., Denk, W., Brecht, M., and Osten, P. (2004) *Proc. Natl. Acad. Sci. U.S.A.* **101,** 18206–18211
22. Paxinos, G., and Franklin, K. B. (2004) *The Mouse Brain in Stereotaxic Coordinates*, Academic Press, Inc., San Diego, CA
23. Prensa, L., and Parent, A. (2001) *J. Neurosci.* **21,** 7247–7260
24. Matsuda, W., Furuta, T., Nakamura, K. C., Hioki, H., Fujiyama, F., Arai, R., and Kaneko, T. (2009) *J. Neurosci.* **29,** 444–453
25. Ungerstedt, U., and Arbuthnott, G. W. (1970) *Brain Res.* **24,** 485–493
26. Lane, E. L., Cheetham, S., and Jenner, P. (2005) *J. Pharmacol. Exp. Ther.* **312,** 1124–1131
27. Dunkley, P. R., Bobrovskaya, L., Graham, M. E., von Nagy-Felsobuki, E. I., and Dickson, P. W. (2004) *J. Neurochem.* **91,** 1025–1043
28. Tank, A. W., Curella, P., and Ham, L. (1986) *Mol. Pharmacol.* **30,** 497–503
29. Fernández, E., and Craviso, G. L. (1999) *J. Neurochem.* **73,** 169–178
30. Lin, A. C., and Holt, C. E. (2008) *Curr. Opin. Neurobiol.* **18,** 60–68
31. Willis, D. E., and Twiss, J. L. (2006) *Curr. Opin. Neurobiol.* **16,** 111–118
32. Jarrott, B., and Geffen, L. B. (1972) *Proc. Natl. Acad. Sci. U.S.A.* **69,** 3440–3442
33. Terada, S. (2003) *Neurosci. Res.* **47,** 367–372
34. Hirokawa, N., Niwa, S., and Tanaka, Y. (2010) *Neuron* **68,** 610–638
35. Zigmond, M. J., Acheson, A. L., Stachowiak, M. K., and Stricker, E. M. (1984) *Arch. Neurol.* **41,** 856–861
36. Cubeddu, L. X., and Hoffmann, I. S. (1982) *J. Pharmacol. Exp. Ther.* **223,** 497–501
37. Håkansson, K., Pozzi, L., Usiello, A., Haycock, J., Borrelli, E., and Fisone, G. (2004) *Eur. J. Neurosci.* **20,** 1108–1112
38. Rice, M. E., and Cragg, S. J. (2008) *Brain Res. Rev.* **58,** 303–313
39. Mosharov, E. V., Larsen, K. E., Kanter, E., Phillips, K. A., Wilson, K., Schmitz, Y., Krantz, D. E., Kobayashi, K., Edwards, R. H., and Sulzer, D. (2009) *Neuron* **62,** 218–229
40. Gordon, S. L., Quinsey, N. S., Dunkley, P. R., and Dickson, P. W. (2008) *J. Neurochem.* **106,** 1614–1623
41. Pothos, E. N., Davila, V., and Sulzer, D. (1998) *J. Neurosci.* **18,** 4106–4118
42. Hefti, F., Enz, A., and Melamed, E. (1985) *Neuropharmacology* **24,** 19–23
43. Fukushima, T., and Nixon, J. C. (1980) Anal. Biochem. **102,** 176–188